Available online at www.sciencedirect.com

SCIENCE DIRECT®

Journal of the Mechanics and Physics of Solids
54 (2006) 887–903

JOURNAL OF THE MECHANICS AND PHYSICS OF SOLIDS

www.elsevier.com/locate/jmps

The effect of water diffusion on the adhesion of organosilicate glass film stacks

Ting Y. Tsui[a,*], Andrew J. McKerrow[a], Joost J. Vlassak[b,**]

[a] *Silicon Technology Development, Texas Instruments Incorporated, Dallas, TX, USA*
[b] *Division of Engineering and Applied Sciences, Harvard University, Cambridge, MA 02138-2901, USA*

Received 18 October 2005; received in revised form 5 December 2005; accepted 8 December 2005

Abstract

Organosilicate glass (OSG) is a material that is used as a dielectric in advanced integrated circuits. It has a network structure similar to that of amorphous silica where a fraction of the Si–O bonds have been replaced by organic groups. It is well known from prior work that OSG is sensitive to subcritical crack growth as water molecules in the environment are transported to the crack tip and assist in rupturing Si–O bonds at the crack tip. In this study, we demonstrate that exposure of an OSG containing film stack to water prior to fracture results in degradation of the adhesion of the film stack. This degradation is the result of the diffusion of water into the film stack. We propose a quantitative model to predict adhesion degradation as a function of exposure time by coupling the results of independent subcritical crack growth measurements with diffusion concentration profiles. The model agrees well with experimental data and provides a novel method for measuring the water diffusion coefficient in film stacks that contain OSG. This study has important implications for the reliability of advanced integrated circuits.
© 2006 Elsevier Ltd. All rights reserved.

Keywords: Organosilicate glass material; Layered material; Water diffusion; Adhesion; Fracture

*Corresponding author. Tel.: +1 972 995 1121.
**Corresponding author. Tel.: +1 617 496 0424.
E-mail addresses: ttsui@ti.com (T.Y. Tsui), vlassak@esag.harvard.edu (J.J. Vlassak).

0022-5096/$ - see front matter © 2006 Elsevier Ltd. All rights reserved.
doi:10.1016/j.jmps.2005.12.004

1. Introduction

In order to improve the performance of advanced integrated circuits, the relative permittivity of insulators used as inter-layer dielectrics in integrated circuits has been reduced from greater than 4.0 for the traditional silicon dioxide to less than 2.5 for dielectrics that are currently used in advanced devices. It is expected that this value will be reduced even further for future generations of integrated circuits. The most common dielectric now in use is organosilicate glass (OSG). This material has a network structure similar to that of amorphous silicon dioxide where a fraction of the Si–O bonds have been replaced by methyl termination groups. The result is an open siloxane network with lower density and dielectric constant than silica. However, one of the drawbacks of introducing the methyl groups is a reduction of the Si–O bond density and hence of the fracture toughness and stiffness of the material. Consequently, the material has a greater propensity for adhesive or cohesive failure modes such as delamination (Lin et al., 2003, 2004; Vlassak et al., 2005) and channel cracking (Tsui et al., 2005).

The Si–O bonds in the OSG make the material susceptible to subcritical crack growth when water is present in the environment (Wiederhorn, 1967; Wiederhorn and Bolz, 1970). This behavior has been investigated extensively for OSG coatings by several researchers (Lin et al., 2003, 2004; Vlassak et al., 2005; Lane et al., 2001; Guyer and Dauskardt, 2004). These researchers measured the adhesion of several capping layers to OSG in various ambient and aqueous conditions using four-point flexure and double cantilever beam adhesion specimens. They demonstrated that the adhesion depends on the partial pressure of water in ambient environments and on the hydroxyl concentration (i.e. on the pH) in aqueous environments. Similar behavior has also been observed for cohesive failure of OSG using a technique based on channel cracking (Tsui et al., 2005). In all these studies, the reactive species (water or OH^-) are transported to the crack tip during the fracture process. Thus far, little or no attention has been paid to the possibility that the reactive species can diffuse into the OSG before fracture takes place if the OSG is exposed to a reactive environment for some period of time. The presence of reactive species in the material is expected to lower the fracture toughness of the OSG with exposure time even if the measurements are made in an inert environment, making this type of measurements fundamentally different from traditional subcritical crack growth experiments. Diffusion of an active species into the film stack then leads to an apparent time-dependent adhesion or fracture toughness that may eventually result in adhesive or cohesive failure of the OSG. This issue has important technological implications for the manufacture and reliability of integrated circuits that contain OSG: During the manufacturing process, integrated circuits are exposed to various reactive environments including aqueous solutions. If the OSG is not sealed at the time of exposure, the reactive species diffuses into the film stack and degrades its resistance to fracture.

The objective of this study is to characterize the effect of water diffusion on the fracture toughness of the interface between OSG and various capping layers. First, a simple quantitative model is presented that links time-dependent adhesion degradation to diffusion of water into the film stack. Then, experimental data are given for the adhesion of various coatings to OSG demonstrating that adhesion indeed degrades with increased exposure time to water. Finally, the rate of adhesion degradation is compared with model predictions. The model suggests a new approach for measuring the diffusion coefficient of water in OSG film stacks.

2. Model

In this section, we develop a quantitative model for the degradation of the adhesion or fracture toughness of a film stack as a result of diffusion of water in the film stack. The geometry we consider in this analysis is appropriate for both double cantilever beam and four-point flexure specimens, test geometries that are often used for measuring the adhesion of thin films (Charalambides et al., 1989, 1990; Ma, 1997; Snodgrass and Dauskardt, 2000). For instance, Fig. 1(a) depicts a schematic illustration of the four-point flexure geometry, which is used for the adhesion measurements in this study. The film stack of interest is sandwiched between two substrates and loaded in bending until delamination occurs. A more detailed description of the technique is given in the experimental section of this paper. Fig. 1(b) provides a transverse cross-sectional view of the specimen and shows the diffusion fronts that develop when the sample is exposed to water. The diffusion process and its effect on the fracture resistance can be described as follows.

Consider an infinitely long film stack sandwiched between two impervious substrates as illustrated schematically in Fig. 1(b). Consider further a Cartesian coordinate system with x-axis perpendicular to the edge of the stack. Assume the film stack is exposed to water at a temperature T along its edges at $x = 0$ and a. Water will then diffuse into the film stack from its edges. This is a simple one-dimensional diffusion problem that results in the following water concentration profile in the OSG strip (Shewmon, 1989):

$$\frac{C(x,t)-C_\mathrm{i}}{C_\mathrm{s}(T)-C_\mathrm{i}} = 1 - \frac{4}{\pi}\sum_{k=0}^{\infty}\frac{1}{2k+1}\sin(\lambda_k x)\exp(-\lambda_k^2 D_{\mathrm{H_2O}} t), \quad \lambda_k = \frac{(2k+1)\pi}{a}, \tag{1}$$

where C_i is the initial water concentration in the OSG, $C_\mathrm{s}(T)$ is the solubility of water in OSG at temperature T, and $D_{\mathrm{H_2O}}$ is the diffusion coefficient of water in the film stack. Implicit to Eq. (1) is the assumption that transport of water molecules from the liquid phase to the surface of the film stack is not rate limiting. For experimental reasons, it is

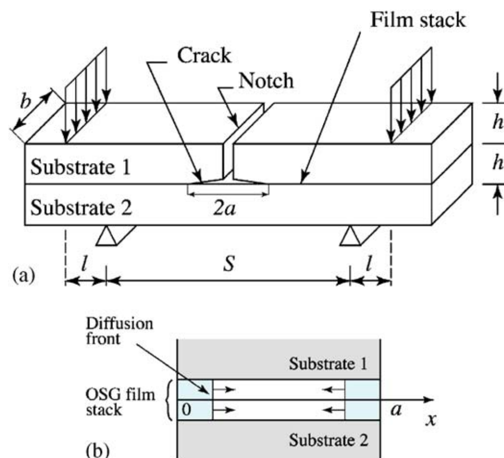

Fig. 1. (a) Schematic of a four-point flexure specimen for adhesion measurements. The OSG film stack is sandwiched between the substrates and is not shown explicitly in the figure. (b) Transverse cross-section of the four-point flexure specimen illustrating the geometry of the diffusion problem.

convenient to reformulate Eq. (1) in terms of water partial pressures. Consider OSG in equilibrium with a water partial pressure p_{H_2O}. Water dissolved in the OSG is in equilibrium with the water vapor outside the OSG according to

$$H_2O(v) \rightleftarrows H_2O(OSG). \tag{2}$$

In equilibrium, the chemical potentials of water inside and outside of the OSG are the same. This leads to the following expression for the equilibrium concentration of water inside the OSG as a function of the partial pressure of water in the environment

$$C = \frac{p_{H_2O}}{\gamma_H^o p_0} \exp\left(-\frac{\Delta\mu_0}{RT}\right) \tag{3}$$

assuming that water dissolved in OSG follows Henry's law. Here, γ_H^o is the activity coefficient, p_0 the reference pressure, and $\Delta\mu_0$ the difference between the standard chemical potential of water inside and outside the OSG with respect to the appropriate reference states. If the OSG is in equilibrium with liquid water at temperature T, it follows that

$$C_s(T) = \frac{p_v}{\gamma_H^o p_0} \exp\left(-\frac{\Delta\mu_0}{RT}\right), \tag{4}$$

where p_v is the water vapor pressure and $C_s(T)$ is the solubility of water in OSG at T. A similar expression can be derived for C_i. Substituting these expressions in Eq. (1) leads to

$$\frac{p_{H_2O}(x,t) - p_i}{p_v - p_i} = 1 - \frac{4}{\pi}\sum_{k=0}^{\infty} \frac{1}{2k+1} \sin(\lambda_k x) \exp(-\lambda_k^2 D_{H_2O} t). \tag{5}$$

The pressure p_i in Eq. (5) is the water partial pressure in equilibrium with the initial water content of the OSG. The pressure p_{H_2O} is the partial pressure that would be in equilibrium with an OSG sample with a uniform water content of $C(x,t)$. Since the concentration of water in the OSG strip changes with time and location, p_{H_2O} is a function of x and t. Eq. (5) is equivalent to Eq. (1), but is expressed in terms of water partial pressures in equilibrium with the appropriate water concentrations. This formulation makes it easier to apply Eq. (5) to the problem at hand, because water partial pressure is a variable that is readily controlled in fracture experiments.

The next step is to relate the fracture resistance of the OSG to the water partial pressure in the environment. It is well known that the resistance to fracture of OSG and other silica-based materials decreases with increasing water partial pressure (Wiederhorn, 1967; Wiederhorn and Bolz, 1970; Lane et al., 2001; Lin et al., 2003, 2004; Vlassak et al., 2005). Fig. 2, for instance, shows the subcritical crack growth velocity in OSG as a function of applied energy release rate for different levels of water partial pressure. At constant crack velocity, the energy release rate indeed decreases with increasing water partial pressure. An analysis of the crack growth kinetics in the reaction-controlled regime (Lawn, 1975; Vlassak et al., 2005) shows that for a given crack velocity

$$G = B - nNRT \ln p_{H_2O} = B - A \ln p_{H_2O} \quad \text{for } G \leqslant G_c, \tag{6}$$

where n is the number of water molecules reacting with a Si–O bond in the OSG, N is the bond density of the OSG in mols per unit area, B is a constant that depends on crack velocity, T is the absolute temperature at which the crack propagates, and G is the energy release rate for that crack velocity.

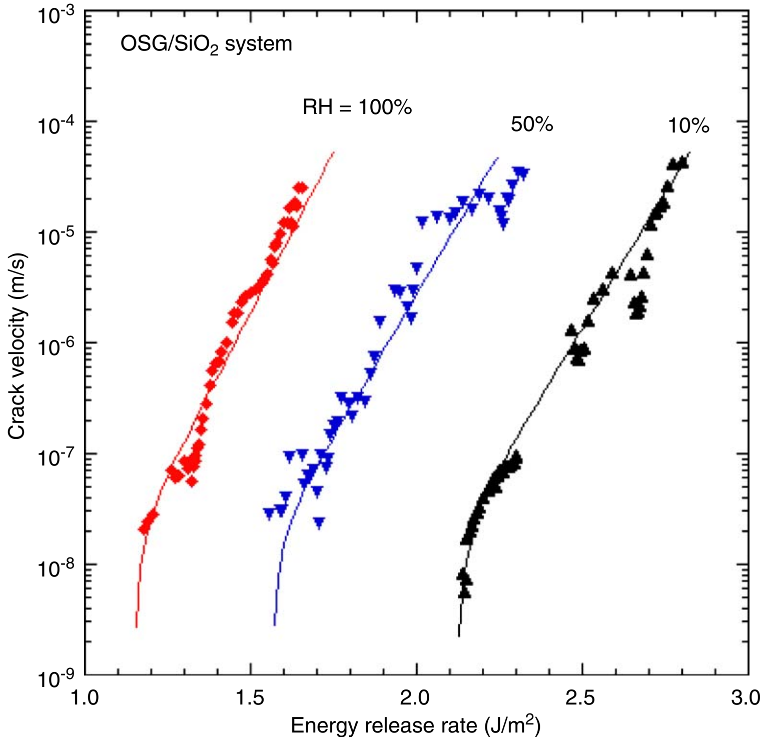

Fig. 2. Subcritical crack growth curves for the OSG/SiO_2 system in an ambient environment with controlled humidity levels (from Vlassak et al., 2005).

Now consider a crack propagating at constant velocity in an OSG film stack sandwiched between two substrates and exposed to water at the edges for a period of time. Assume the crack propagates parallel to the substrate as it would for a four-point flexure or double cantilever beam fracture specimen, i.e. the crack propagates into or out of the plane of Fig. 1(b). The water content of the OSG now varies along the crack front as described by Eqs. (1) or (5). Since the crack travels at a constant velocity, the energy release rate must also vary along the crack front, unless the water content is uniformly distributed throughout the OSG film. It follows then that the crack front must be curved, with the sign of the curvature determined by the ratio p_i/p_v. The energy release rate at a given point along the crack front required to drive the crack at constant velocity is then given by Eq. (6), where p_{H_2O} is the water partial pressure in equilibrium with the local water content, i.e.

$$G(x,t) = B - A\ln\left\{p_i + (p_v - p_i)\left(1 - \frac{4}{\pi}\sum_{k=0}^{\infty}\frac{1}{2k+1}\sin(\lambda_k x)\exp(-\lambda_k^2 D_{H_2O}t)\right)\right\} \tag{7}$$

by combining Eqs. (5) and (6). The average energy release rate along the crack front, i.e. the quantity that is measured macroscopically, is then

$$G_a(t) = \frac{1}{a}\int_0^a G(x,t)\,dx,$$

$$= B - \frac{A}{a}\int_0^a \ln\left\{p_\mathrm{i} + (p_\mathrm{v} - p_\mathrm{i})\right.$$
$$\left.\times\left(1 - \frac{4}{\pi}\sum_{k=0}^{\infty}\frac{1}{2k+1}\sin(\lambda_k x)\exp(-\lambda_k^2 D_{\mathrm{H_2O}} t)\right)\right\}\mathrm{d}x. \tag{8}$$

After substituting $x = a\xi$, Eq. (8) can be written as

$$G_a(t) = B - A(\ln p_\mathrm{v} + \Phi(\gamma, \tau)), \tag{9}$$

where

$$\Phi(\gamma,\tau) = \int_0^1 \ln\left\{\gamma + (1-\gamma)\left(1 - \frac{4}{\pi}\sum_{k=0}^{\infty}\frac{1}{2k+1}\sin((2k+1)\pi\xi)\exp(-(2k+1)^2\pi^2\tau)\right)\right\}\mathrm{d}\xi \tag{10}$$

and

$$\gamma = \frac{p_\mathrm{i}}{p_\mathrm{v}} \quad \text{and} \quad \tau = \frac{D_{\mathrm{H_2O}} t}{a^2}. \tag{11}$$

The function $\Phi(\gamma, \tau)$ represents the time-dependence of the macroscopic energy release rate and is readily evaluated numerically. Fig. 3 shows $\Phi(\gamma, \tau)$ as a function of the normalized time τ and for various values of the normalized initial water content γ of the OSG. It should be noted that the constants A and B can be determined by performing sub-critical

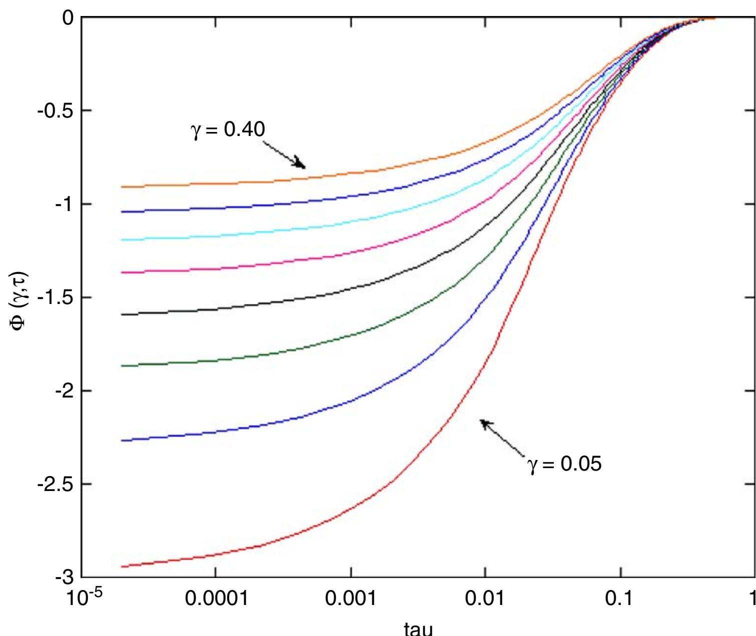

Fig. 3. $\Phi(\gamma, \tau)$ as a function of the normalized time τ for different initial water content ratios of the film. Curves are shown for γ increments of 0.05.

fracture measurements in environments with different water partial pressures. Eq. (9) suggests the following simple method for determining the diffusion coefficient D_{H_2O}: Plot the experimental value of the crack extension force as a function of the logarithm of the time that the OSG has been exposed to water. The shape of this curve should be similar to the shape of the curve obtained from Eq. (9) using the appropriate values of γ, A, and B, but shifted along the time axis. The shift along the time axis is a measure of the value of the diffusion coefficient of water in OSG and the diffusion coefficient can be extracted using Eq. (11).

3. Experimental procedure

Organosilicate glass thin films (OSG) with a thickness of 420 nm were deposited on 200 mm diameter bare silicon wafers at 400 °C by means of plasma-enhanced chemical vapor deposition (PECVD). The precursor gases used in the deposition were 3, 5, 7-tetra-methylcyclo-tetrasiloxane (TMCTS), carbon dioxide, and oxygen. The OSG density was measured with Rutherford Backscattering Spectrometry (RBS) and is approximately 1.2 g/cm^3; the relative dielectric constant of the OSG was 3.0. The precise chemical composition and mechanical properties of the OSG have been reported in previous studies by Vlassak and coworkers (Lin et al., 2003, 2004; Xiang et al., 2004; Vlassak et al., 2005). As-deposited OSG coatings have a porosity of approximately 8% as measured using X-ray reflectometry and ellipsometry. Here, the effect of water diffusion on the adhesion between OSG and four different capping materials is investigated—tantalum, tantalum nitride (TaN_x), silicon nitride (SiN_x), and silicon dioxide (TEOS-SiO_2). The last three capping layers are identical to those studied by Vlassak and coworkers (Lin et al., 2003, 2004; Vlassak et al., 2005). The SiO_2 and SiN_x coatings were deposited at 400 °C using PECVD. The TaN_x coatings were deposited using reactive sputtering, followed by an in situ sputter deposition of a thin copper coating. The Ta coatings were sputter-deposited. The film thicknesses for the various film stacks are listed in Table 1; the substrate thickness was $730 \pm 10\,\mu m$.

The adhesion energy of all the samples was measured using the four-point flexure technique (Charalambides et al., 1989, 1990; Ma, 1997). Adhesion samples were prepared by cleaving 200 mm silicon substrates into 12 mm × 60 mm strips. These strips were then bonded face-to-face using epoxy and cured for one hour at 120 °C. After curing the epoxy, the samples were pre-notched using a diamond saw. The samples were then loaded in pure bending until a crack nucleated at the notch and propagated into the film stack selecting the weakest interface in the stack. In the four-point flexure geometry, the energy release

Table 1
Film stacks investigated in this study

Film stack	Thicknesses (nm)
OSG/SiO_2	400/200
	400/1600
	3000/1600
OSG/SiN_x	400/200
OSG/Ta	400/10–20
OSG/TaN_x/Cu	400/10–20/100

rate does not depend on crack length. As a result, an interfacial crack propagating at constant velocity results in a plateau in the load–displacement curve. If P is the constant load at which the crack propagates, the corresponding energy release rate G is given by (Charalambides et al., 1990)

$$G = \frac{21P^2 l^2 (1 - v^2)}{16Eb^2 h^3}, \tag{12}$$

where E and v are the elastic modulus and Poisson's ratio of the Si substrate, l the distance between the inner and outer loading pins in the four-point flexure set-up, b the width of the specimen, and h the substrate thickness (cf. Fig. 1(a)). For each capping material, one group of samples was tested immediately after the epoxy was set. The rest of the specimens were submerged in de-ionized water ($T = 24 \pm 2\,^{\circ}\mathrm{C}$ and $100\,^{\circ}\mathrm{C}$) and tested after exposing them for specific periods of time. Unless stated otherwise, all adhesion measurements were conducted in an ambient environment with $45 \pm 5\%$ relative humidity and a temperature of $24 \pm 2\,^{\circ}\mathrm{C}$. The crack velocity was approximately $60\,\mu\mathrm{m/s}$ for all measurements.

4. Results and discussion

4.1. The effect of water diffusion on adhesion energy

Fig. 4 shows the adhesion energy between the OSG and the various capping layers as a function of submersion time in de-ionized water at 24 °C. Each data point represents the average of at least five measurements and the error bars correspond to one standard deviation. X-ray photoelectron spectroscopy (XPS) of the fractures surfaces reveals that the crack path is located inside the OSG at a distance of approximately 5–10 nm from the interface for the SiN_x, Ta, and TaN_x-capped samples. The adhesion energy of the Ta-capped samples is larger than for the other samples because a pre-deposition plasma clean was used to remove contaminants from the OSG surface of these samples and this plasma clean densifies the OSG near the surface. For the OSG/SiO_2 samples, by contrast, the XPS results show that the delamination occurred at the interface. This is consistent with observations reported by Vlassak et al. (2005). It is evident from Fig. 4 that the adhesion of each of the four film stacks degrades with increasing exposure time. Annealing experiments on the OSG/SiN_x film stack further demonstrate that the adhesion can be fully recovered to the pre-exposure value by vacuum-baking the film stack for three hours at 250 °C. This observation implies that the adhesion degradation is reversible as long as fracture does not occur prior to diffusion of water, i.e. the Si–O bonds do not react with water until they are stressed.

In order to eliminate the possibility that the time-dependent adhesion degradation is caused by changes in the mechanical properties of the epoxy as a result of the absorption of water, OSG/SiO_2 samples with different bi-layer thicknesses were tested: 200 nm SiO_2/420 nm OSG, 1600 nm SiO_2/420 nm OSG, and 1600 nm SiO_2/3000 nm OSG. If energy dissipation in the epoxy contributes significantly to the experimental adhesion values, the different film stacks should yield different adhesion values, because the stress distribution at the crack tip depends on the thicknesses of the films in the stack (Suo and Hutchinson, 1989). As illustrated in Fig. 5, this is clearly not the case: The initial adhesion values and the rates of degradation are indistinguishable within experimental scatter for the different

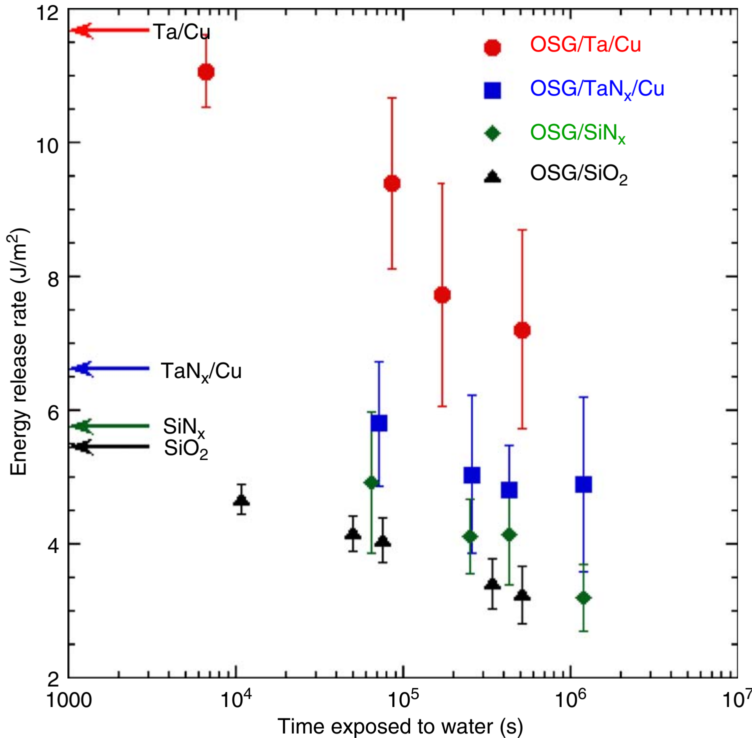

Fig. 4. Adhesion energy of several materials systems as a function of time exposed to water at 24 °C. The OSG thickness is 420 nm for all systems; capping layer thicknesses are given in Table 1. The arrows mark the adhesion energies prior to exposure to water.

film stacks. This indicates that the adhesion degradation is related to changes that take place in the OSG at or near the delaminating interface.

Fig. 6 shows the adhesion energy as a function of soak time for SiO_2-capped OSG coatings soaked in de-ionized water at 100 °C. Each data point is the mean of at least five measurements and the error bars represent one standard deviation. Again, there is no significant difference between specimens with 200 or 1600 nm of SiO_2, indicating that any softening of the epoxy that may occur as a result of water diffusion does not affect the measurements. It is evident from the data in Fig. 6 that degradation occurs significantly faster at 100 °C than at room temperature—the degradation process is accelerated by a factor of twenty or so.

4.2. The effect of testing environment on fracture toughness

In order to evaluate the effect of water vapor in the testing environment on the degradation of the adhesion, several OSG samples coated with SiO_2 were exposed to de-ionized water at room temperature for various periods of time and tested under three different conditions of relative humidity: $5 \pm 3\%$, $45 \pm 5\%$, and $98 \pm 2\%$. Fig. 7 shows the fracture toughness of these samples as a function of the partial pressure of water in the testing environment. Two trends are immediately observed: The fracture toughness

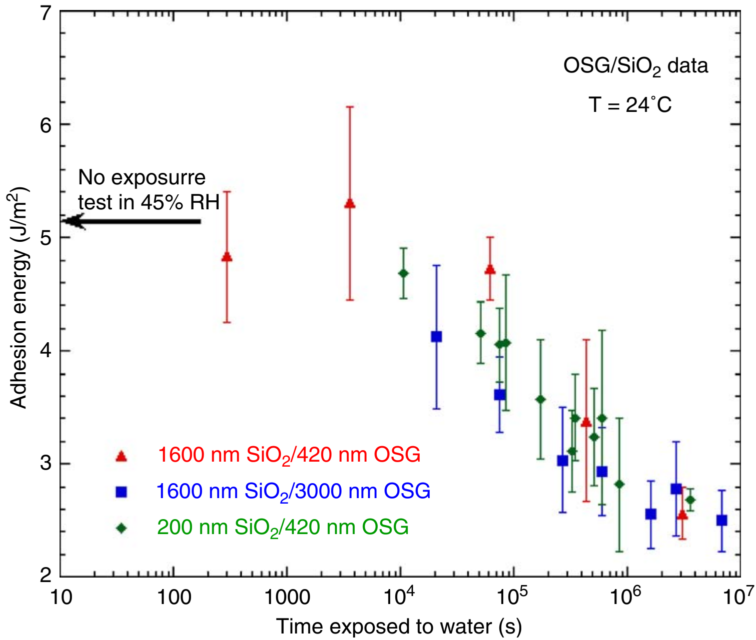

Fig. 5. Adhesion energy of the OSG/SiO_2 system as a function of time exposed to water at 24 °C for various values of OSG and SiO_2 layer thickness. The arrow marks the adhesion energy prior to exposure to water.

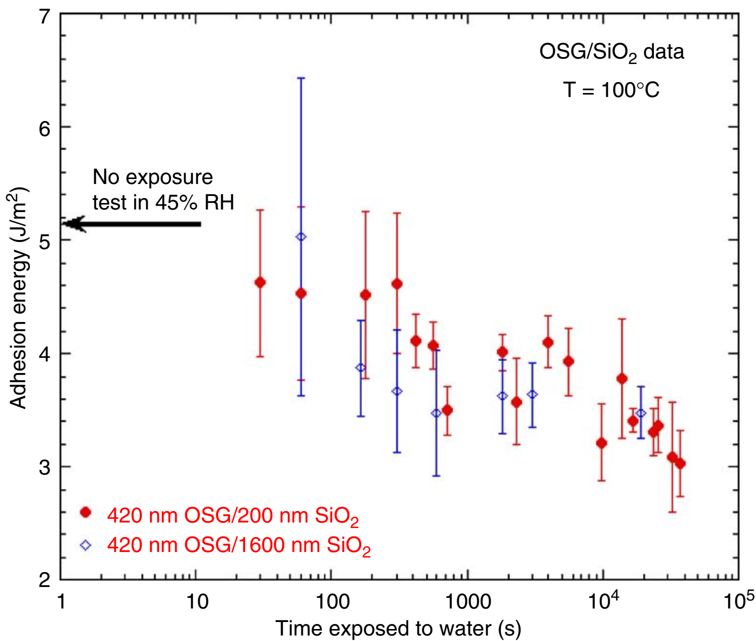

Fig. 6. Adhesion energy of the OSG/SiO_2 interface as a function of time exposed to water at 100 °C for a 420 nm OSG film with a 200 nm SiO_2 capping layer. The arrow marks the adhesion energy prior to exposure to water.

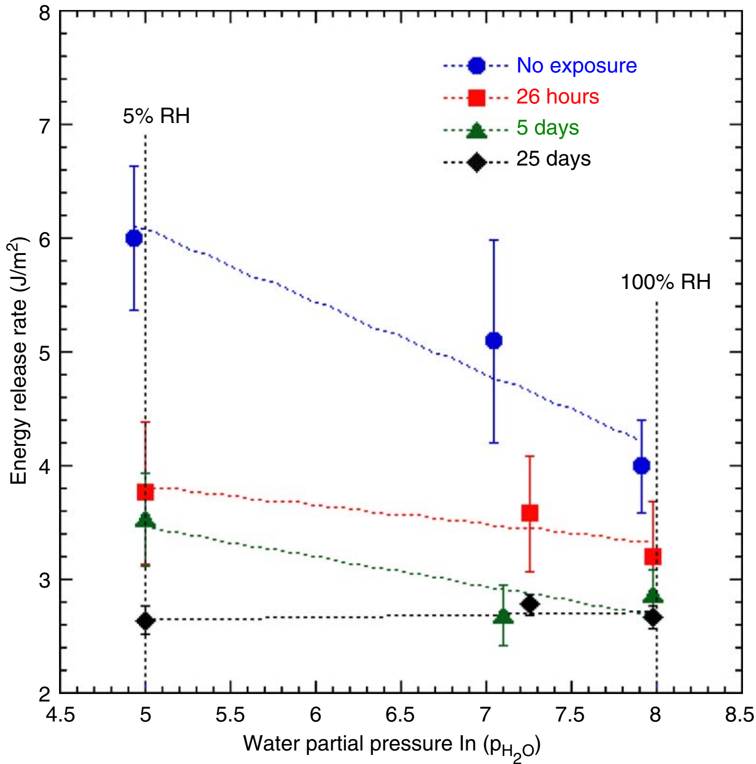

Fig. 7. Adhesion energy of the OSG/SiO_2 interface as a function of water partial pressure in the testing environment after exposure to water at 24 °C for various periods of time. Partial pressures are given in Pascal.

decreases with increasing exposure time. This trend of course agrees with the results in Figs. 4 and 5. Furthermore, the fracture toughness decreases with increasing water partial pressure in the environment in agreement with previous reports (Wiederhorn, 1967; Lane et al., 1999; Vlassak et al., 2005). The question then arises how to separate both effects. The crack velocity at which transport of water molecules from the environment to the crack tip becomes important can be estimated from (Lawn, 1993; Vlassak et al., 2005)

$$v_t = \frac{64(1-v^2)Gp_{H_2O}}{3\pi nNE\sqrt{2\pi mkT}\ln(l/b)}, \tag{13}$$

where p_{H_2O} is the water partial pressure in the environment, m the molecular mass of water, l is the mean free path length of a water molecule, and n the number of molecules adsorbed per broken bond. G is the mode I energy release rate, E and v are Young's modulus and Poisson's ratio, and b the bond length. If a crack propagates at a velocity larger than v_t, water molecules do not have time to diffuse to the crack tip and the fracture behavior is determined by the water molecules already present in the OSG as a result of diffusion during the water soak. If a crack propagates at a velocity smaller than v_t, water from the environment can reach the crack tip and lower the resistance of the material to fracture.

The velocity calculated from Eq. (13) is several times smaller than the experimental crack velocity for the measurements made at a relative humidity of 5%, but is larger for measurements performed at 98% relative humidity. Consequently, the measurements at 5% relative humidity are independent of the environmental conditions and any changes in the adhesion as a function of soaking time reflect changes in the water content of these specimens as a result of diffusion during the soak.

It should be noted that the data in Fig. 7 also indicate there is an asymmetry in the transport of water molecules to and from the crack tip: once the specimens are saturated with water, the adhesion energy is approximately $2.7\,J/m^2$, *independent* of the environmental conditions. However, for specimens tested at 5% relative humidity, one might reasonably expect water to diffuse away from the crack tip, thus lowering the water concentration at the crack tip and increasing the adhesion energy. This is clearly not the case. This observation indicates that transport away from the crack tip is more difficult than transport to the crack tip, possibly because water molecules need to desorb from the crack surface before they can diffuse away.

4.3. Model and discussion

The diffusion model presented in the previous section can be used to describe the adhesion data in Figs. 4–6. In principle, Eq. (9) could be fitted directly to the data in these figures using A, B, γ and D as fitting parameters. It is possible, however, to obtain values for some of these parameters from independent measurements. Fig. 8, for instance, shows the energy release rate as a function of water partial pressure for a crack velocity of $60\,\mu m/s$ for OSG coatings with three different capping layers. The data used to construct this graph was obtained from subcritical crack growth measurements reported by Vlassak et al. (2005) for OSG coatings that are very similar to the coatings used in this investigation. Since the crack velocity of interest is relatively large, the reaction-controlled regimes of the subcritical crack growth curves were extrapolated to the appropriate crack velocity. This was done to ensure that slow transport of water molecules to the crack tip would not lead us to overestimate the effect of water partial pressure on energy release rate. It is evident from Fig. 8 that within experimental scatter the constant $A = nNRT$ is the same for the three film stacks in the figure. The constants B and γ can then be determined from the results in Fig. 7: Specimens that are fully saturated with water at room temperature yield an energy release rate of $2.7\,J/m^2$, as-fabricated specimens yield a value of $6\,J/m^2$. Application of Eq. (6) to these results along with the value of A from Fig. 8 yields values for B and $p_i = \gamma p_v$. Values of A, B, and γ used in the model are tabulated in Table 2. The initial water content of the samples is very low as evidenced by the small value of γ. This is consistent of the fact that the OSG films are heated to $400\,^\circ C$ in UHV immediately prior to the PECVD SiO_2 deposition. Fig. 9 shows the experimental data for the OSG/SiO_2 system along with the results obtained from the diffusion model, in which the diffusion coefficient was used as a fitting parameter. Agreement between the experimental data and the model calculations is very good, with the exception of the initial part of the curve where the model slightly over-predicts the energy release rates. This discrepancy arises because these measurements were conducted under ambient conditions with a relative humidity of 45%. Water molecules that are transported to the crack tip during the measurement weaken the Si–O bonds and lower the energy release rate. The same measurements performed in an inert N_2 atmosphere are in much better agreement

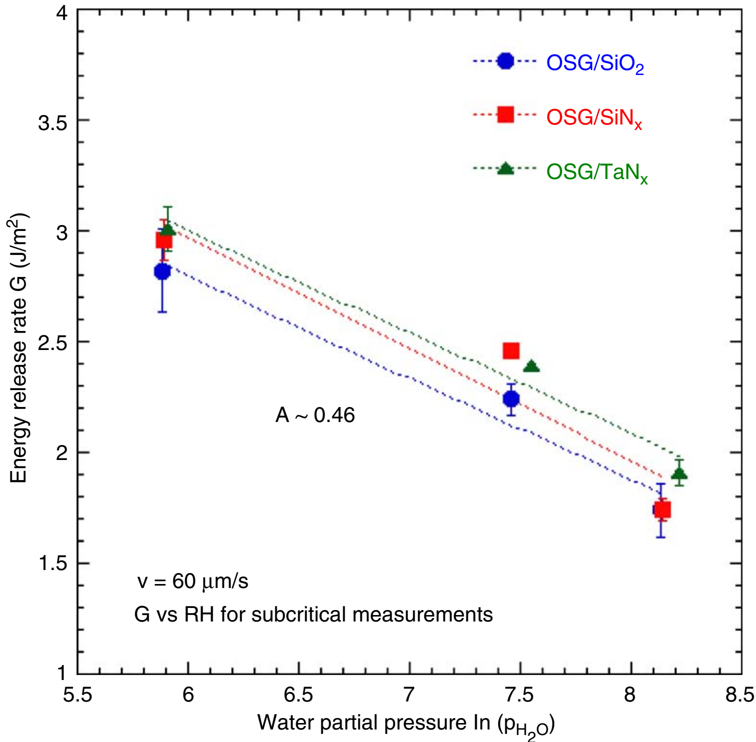

Fig. 8. Energy release rate to drive an interfacial crack at a given velocity as a function of water partial pressure in the testing environment. The results were obtained from subcritical crack growth measurements on OSG with several capping layers reported by Vlassak et al. (2005). Because of the large crack velocity, the reaction-controlled regimes of the subcritical crack growth curves were extrapolated to the appropriate crack velocity to avoid transport-control effects. Partial pressures are given in Pascal.

Table 2
Coefficients relating energy release rate and water partial pressure (in Pa) for the OSG/SiO_2 system and for a crack velocity of 60 μm/s

A	0.46 J/m^2
B	6.27 J/m^2
γ	0.0006

with the model as indeed illustrated in the figure. At longer exposure times, the effect of the environment becomes less important. This is evident in Fig. 7 as well. The diffusion coefficient obtained from the model is $1.4 \times 10^{-7}\,\mathrm{cm}^2/\mathrm{s}$.

The model can also be applied to the specimens that were exposed to water at elevated temperature (Fig. 6). Because the temperatures of the diffusion experiment (T_D) and the adhesion measurements (T_A) are now different, some care needs to be exercised with respect to the partial pressures used in Eqs. (5) and (6). The pressure in Eq. (6) is the water partial pressure in equilibrium with the OSG at the temperature of the adhesion measurement; the partial pressures in Eq. (5) are by definition those in equilibrium with the

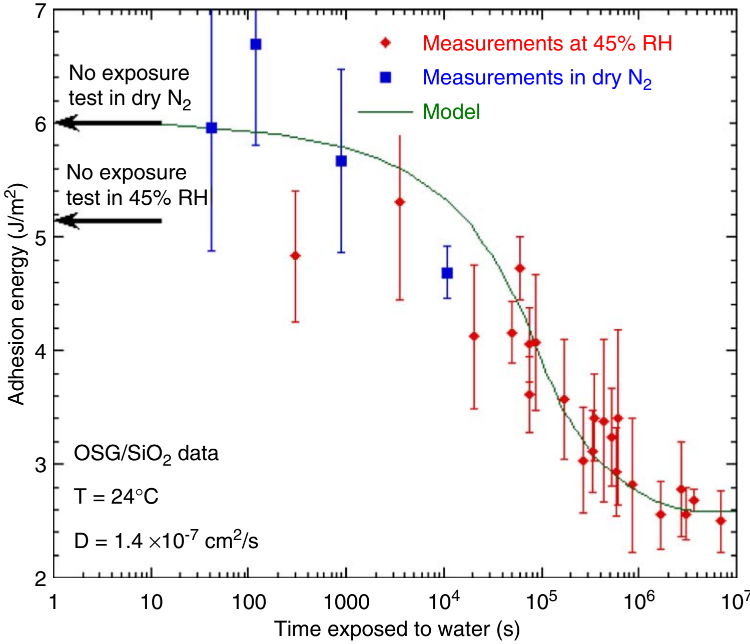

Fig. 9. Adhesion energy of the OSG/SiO_2 system as a function of time exposed to water at 24 °C. The solid line represents the diffusion model. The arrows represent energy release rates for as-fabricated specimens tested in either dry N_2 or at a relative humidity of 45%. All adhesion measurements were made at 24 °C.

various water concentrations at the temperature of the diffusion experiment. For a given water concentration in the OSG, the partial pressures at these temperatures are related by the equation

$$p^{T_A} = p^{T_D} \frac{C_s^{T_D}}{C_s^{T_A}} \frac{p_v^{T_A}}{p_v^{T_D}}, \tag{14}$$

where $C_s^{T_D}$ and $C_s^{T_A}$ are the solubility of water at T_D and T_A, respectively. This equation follows directly from Eq. (3) applied at the corresponding temperatures and water concentrations. If the solubility of water is temperature independent, the right-hand side of Eq. (14) is simply the ratio of the water vapor pressures at the relevant temperatures. Taking into account the effect of different temperatures, Eq. (9) becomes

$$G_a(t) = B - A\left[\ln\left(\frac{C_s^{T_D}}{C_s^{T_A}} p_v^{T_A}\right) + \Phi(\gamma,\tau)|_{T^D}\right], \tag{15}$$

where

$$\Phi(\gamma,\tau)|_{T^D} = \Phi\left(\frac{p_i^{T_A}}{p_v^{T_A}} \frac{C_s^{T_A}}{C_s^{T_D}}, \tau\right) \tag{16}$$

and τ is evaluated using the diffusion coefficient at T_D. It is interesting to note that the $G_a(t)$ function now depends on the water solubility ratio $C_s^{T_A}/C_s^{T_D}$. For small temperature changes such as those in this study, one can expect this ratio to be close to unity. In

principle, however, it may be possible to obtain information on the solubility of water from a measurement of $G_a(t)$: It is evident from Eq. (15) that the saturation value of the energy release rate shifts up or down with the value of $C_s^{T_A}/C_s^{T_D}$. Fig. 10 shows the experimental energy release rates measured for the OSG/SiO_2 system at room temperature as a function of exposure time to water at 100 °C. The solid line represents Eq. (15), in which the diffusion coefficient at 100 °C was used as a fitting parameter—all other parameters are the same as before. Agreement between model and experimental data is very encouraging, especially for the measurements obtained in dry N_2. The corresponding diffusion coefficient is $D = 2.6 \times 10^{-6}\,cm^2/s$. It is evident that the energy release rate in the high-temperature experiments has not yet saturated at the end of the experiments and it is thus difficult to determine if there is increased water solubility at this temperature. For simplicity, the water solubility ratio in the model was taken equal to one. Small changes in solubility do not, however, result in a significant change of the diffusion coefficient obtained from the model, nor does the diffusion coefficient depend sensitively on the precise values of A and B. The activation energy calculated from the temperature dependence of the diffusion coefficient is estimated to be 0.37 eV.

The experimental values of the diffusion coefficient are relatively large implying fast transport of water. From the experiments it is not possible to determine unambiguously whether diffusion takes place primarily along the interface or through the bulk of the coating. Since transport is fast, one might assume at first that it occurs primarily along the interface between the OSG and the SiO_2. The data in Fig. 4, however, show that the adhesion energy degrades at approximately the same rate for different materials systems

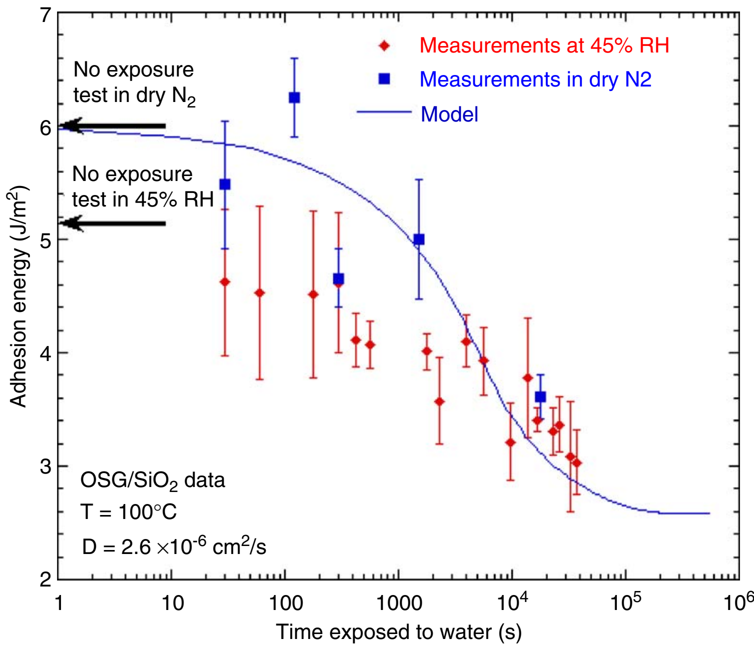

Fig. 10. Adhesion energy of the OSG/SiO_2 system as a function of time exposed to water at 100 °C. The solid line represents the diffusion model. The arrows represent energy release rates for as-fabricated specimens tested in either dry N_2 or at a relative humidity of 45%. All adhesion measurements were made at 24 °C.

and hence different interfaces. This makes it less likely that transport occurs mainly along the interface. Given the porosity of the OSG material and its open network structure, transport through the bulk of the film indeed cannot be excluded. Literature data on the diffusion of water in OSG are scarce since most diffusion experiments are performed using organic solvents such as toluene or ethanol (Shamiryan and Maex, 2003; Worsley et al., 2005). These solvents have a refractive index sufficiently different from OSG that diffusion fronts can be tracked using optical microscopy. Diffusion coefficients of 1×10^{-7} and $0.8 \times 10^{-7}\,cm^2/s$ have been reported for toluene and ethanol, respectively, in an OSG material with 7% porosity (Shamiryan and Maex, 2003). Assuming that diffusion of these solvents is representative for the behavior of water, agreement with our results is quite good.

5. Conclusions

It is well known from prior work that OSG is sensitive to subcritical crack growth as water molecules in the environment are transported to the crack tip and assist in rupturing Si–O bonds at the crack tip. In this study, we have demonstrated that exposure of an OSG containing film stack to water prior to fracture results in degradation of the adhesion of the film stack. This degradation is the result of the diffusion of water into the OSG film stack and is fully reversible with an appropriate heat treatment. We have developed a quantitative model to predict the adhesion degradation as a function of exposure time by coupling the results of subcritical crack growth measurements with diffusion concentration profiles. The model agrees well with experimental data and provides a novel method for measuring the water diffusion coefficient in the film stack. This study has important implications for the reliability of advanced integrated circuits where OSG is used as a dielectric.

Acknowledgments

The authors would also like to express their gratitude to Rhida Dalmacio and Darrell Ingram for assistance with sample preparation and to the Kilby Wafer Fabrication Center for deposition of the coatings. Helpful discussions with Dr. Kelly Taylor are gratefully acknowledged by TYT and AJM. Additional thanks go to the SiTD management at Texas Instruments for their support of the mechanical reliability program. One of the authors (JJV) would like to acknowledge support from the Semiconductor Research Corporation (Task ID 1339.001).

References

Charalambides, P.G., Lund, J., Evans, A.G., McMeeking, R.M., 1989. A test specimen for determining fracture resistance of bimaterial interfaces. J. Appl. Mech. 56, 77–82.

Charalambides, P.G., Cao, H.C., Lund, J., Evans, A.G., 1990. Development of a test method for measuring the mixed mode fracture resistance of bimaterial interfaces. Mech. Mater. 8, 269–283.

Guyer, P.E., Dauskardt, R., 2004. Fracture of nanoporous thin-film glasses. Nat. Mater. 3 (1), 53–57.

Lane, M., Dauskardt, R., Ma, Q., Fujimoto, H., Krishna, N., 1999. Subcritical debonding of multilayer interconnect structures: temperature and humidity effects. Mater. Res. Soc. Proc. 563, 251.

Lane, M.W., Snodgrass, J.M., Dauskardt, R.H., 2001. Environmental effects on interfacial adhesion. Microelectron. Reliabil. 41, 1615–1624.

Lawn, B.R., 1975. Atomistic model of kinetic crack growth in brittle solids. J. Mater. Sci. 10, 469–480.

Lawn, B., 1993. Fracture of Brittle Solids, second ed., Cambridge University Press, Cambridge.

Lin, Y., Vlassak, J.J., Tsui, T.Y., McKerrow, A.J., 2003. Environmental effects on subcritical delamination of dielectric and metal films from organosilicate glass (OSG) thin films. Mater. Res. Symp. Proc. 766, E9–4.

Lin, Y., Vlassak, J.J., Tsui, T.Y., McKerrow, A.J., 2004. Subcritical delamination of dielectric and metal films from low-k organosilicate glass (OSG) thin films in buffered pH solutions. Mater. Res. Symp. Proc. 795, 93–98.

Ma, Q., 1997. A four-point bending technique for studying subcritical crack growth in thin films and at interfaces. J. Mater. Res. 12 (3), 840–845.

Shamiryan, D., Maex, K., 2003. Solvent diffusion in porous low-k dielectric films. Mater. Res. Soc. Proc. 766, 229–234.

Shewmon, P., 1989. Diffusion in Solids. The Minerals, Metals, and Materials Society, Warrendale, PA.

Snodgrass, J.M., Dauskardt, R.H., 2000. The effect of fatigue on the adhesion and subcritical debonding of benzocyclobutene/silicon dioxide interfaces. Mater. Res. Soc. Proc. 612, D1.3.

Suo, Z., Hutchinson, J.W., 1989. Sandwich test specimens for measuring interface crack toughness. Mater. Sci. Eng. A 107, 135–143.

Tsui, T.Y., McKerrow, A.J., Vlassak, J.J., 2005. Constraint effects on thin film channel cracking behavior. J. Mater. Res. 20 (9), 2266–2273.

Vlassak, J.J., Lin, Y., Tsui, T.Y., 2005. Fracture of organosilicate glass thin films: environmental effects. Mater. Sci. Eng. A 391, 159–174.

Wiederhorn, S.M., 1967. Influence of water vapor on crack propagation in soda-lime glass. J. Am. Ceram. Soc. 50, 407–415.

Wiederhorn, S.M., Bolz, L.H., 1970. Stress corrosion and static fatigue of glass. J. Am. Ceram. Soc. 53 (10), 543–548.

Worsley, M.A., Roberts, M., Bent, S.F., Gates, S.M., Shaw, T., Volksen, W., Miller, R., 2005. Detection of open or closed porosity in low-k dielectrics by solvent diffusion. Microelectron. Eng. 82, 113–118.

Xiang, Y., Tsui, T.Y., Vlassak, J.J., McKerrow, A.J., 2004. Measuring the elastic modulus and ultimate strength of low-k dielectric materials by means of the bulge test. IITC Proceedings, 133–135.